Space Sci Rev (2009) 148: 455–474
DOI 10.1007/s11214-009-9565-y

The Microscope Mission and Its Uncertainty Analysis

Pierre Touboul

Received: 10 December 2008 / Accepted: 7 July 2009 / Published online: 29 July 2009

Abstract The accurate test of the Universality of Free Fall may demonstrate a violation of Einstein Equivalence Principle (EP) as most attempts of Grand Unification theories seem to conduct. The MICROSCOPE space mission aims at an accuracy of 10^{-15} with a small drag free satellite and a payload based on electrostatic inertial sensors. The two test-masses made of Platinum and Titanium alloys are forced to follow accurately the same orbit. The sets of surrounding electrodes carried by gold coated silica parts allows the generation of electrical fields and electrostatic pressures on the masses. Common forces and torques are exploited to control the satellite drag compensation system and its fine inertial or rotating pointing. Difference in the force along the Earth gravity monopole is accurately measured and interpreted for the test. After a short presentation of the mission and the instrument, most of the relevant parameters to the experiment performance are detailed as well as the associated technologies to reach the expected levels of accuracy. Present error budgets confirm the test expected accuracy of better than 10^{-15}.

Keywords Equivalence principle · Universality of free fall · MICROSCOPE space mission · Electrostatic inertial sensors · Space accelerometers

1 Introduction

The accurate test of the universality of free fall, as depicted by Galileo and considered by Newton, is today much than the verification of this well known property. The violation of the universality of free fall leads to the violation of the Equivalence Principle (EP), fundamental basis of the Einstein General Relativity. Einstein, himself considered this symmetry as enacted by the experimental results: "*The ratio of the masses of two bodies is defined in two ways which differ from each other fundamentally... The equality of these two masses, so*

P. Touboul (✉)
Physics and Instrumentation Department, ONERA, BP 72, 92322 Châtillon Cedex, France
e-mail: pierre.touboul@onera.fr
url: http://www.onera.fr

differently defined, is a fact which is confirmed by experiments... The possibility of explaining the numerical equality of inertia and gravitation by the unity of their nature, gives to the general theory of relativity, according to my conviction, such a superiority over the conception of classical mechanics..." (Einstein 1922). Furthermore, the Equivalence Principle lies at the foundation of other metric theories of gravity like Brans and Dicke one (Brans and Dickes 1961; Will 1985). Today, most attempts of Grand Unification like String theory and M-theory allow the violation of this principle (Damour 1996, Damour et al. 2002), introducing in particular scalar fields, while the experimental investigation of quantum gravity does appear directly very weakly accessible, see for instance the Plank length of 1.6×10^{-35} m. The test of the Equivalence Principle is thus more then the test of general relativity but also the look for new experimental results as the necessary support of new theory. In addition, supersymmetry might be confirmed by the results which should be obtained in the near future with CERN LHC and new particles to be taken into consideration (Feldman et al. 2008).

The test of the universality of free fall with ultimate accuracy is then an important challenge regarding also the dark matter query. In this context, many efforts have been payed to perform important progress in the performance of ground tests (Schäfer 2003). Previous results have been obtained in the last decade with torsion balance and small laboratory bodies up to an accuracy of composition-dependant relative acceleration of $+/-4 \times 10^{-13}$ (Baessler et al. 1999). Moon laser ranging and the comparison of the Earth and Moon relative motions in the Sun field lead to the same order of performance (Williams et al. 1996). Concerning the laser ranging of passive satellite, no better performance can be expected in the near future (Iorio 2007).

Recent results have been obtained with continuously rotating balance in order to better reject the disturbances from the laboratory activities and the gravity gradient fluctuations: Eötvös parameter between Beryllium and Titanium has been evaluated to $(0.3+/-1.8) \times 10^{-13}$ (Schlamminger et al. 2008).

Other developments have been undertaken to increase the performance of such apparatus by magnetic superconducting levitation of the balance rotor in order to suppress the disturbances introduced by the 20 μm tungsten wire (Hammond et al. 2007). Reduction of the thermal environment has also been considered by implementing the apparatus in a helium Dewar (Newman 2001). New laser ranging telescope is also under implementation (Currie et al. 2008). In the same time, the MICROSCOPE space mission has been conceived and designed in order to reach a test accuracy level of 10^{-15}. The definition of the mission takes advantage of existing space accelerometers with dedicated configurations and technologies for ultimate performances (Touboul et al. 2001). This space experiment exploits the specific soft environment that can be reached on board a drag free satellite with very weak residual accelerations and thermal fluctuations, and considers the possibility of a long duration experiment in a free fall laboratory when in orbit around the Earth.

2 The MICROSCOPE Space Experiment

The MICROSCOPE space mission has been selected since several years in the Cnes scientific program and the production of the satellite payload is now undertaken. The satellite is a rather small satellite of 200 kg that has been fully defined and dedicated to the MICROSCOPE fundamental physics experiment. The constraints of the available mass (35 kg), volume and power (40 W) for the dedicated scientific payload have been considered from the initial definition leading to a non cryogenic experiment, with a limited couple of tested materials, and a test performance that should be even better in

Table 1 Proof mass properties

Material	N/μ	Z/μ	$(N+Z)/\mu$	$(N-Z)/\mu$
PtRh10	0.59613	0.40357	0.999704	0.192555
TA6V	0.54197	0.46061	1.002588	0.081358

the future but with more complex mission, satellite and instrument (Sumner et al. 2007; Lafargue et al. 2002).

The concept of this space experiment is a basic free-fall test around the Earth, with the availability of long measurement duration, reduced test-mass disturbing accelerations, very precise instruments optimised for micro-gravity operation and the Earth gravity source signal modulated by the orientation of the rotating instrument leading to reach a precision of 10^{-15}. In fact, two masses of different composition will be precisely positioned on the same orbit. In absence of Equivalence Principle violation, the two masses, submitted to the same Earth gravity field, will continue on the same common trajectory. The satellite which carries the instruments including the masses will be controlled to follow this common trajectory by acting the thrusters of its propulsion system, protecting the masses from Earth and Sun radiation pressures and from residual atmospheric drag. More precisely, the motion of the two masses will be accurately measured with respect to the same on board instrument reference frame and servo-controlled thanks to electrostatic actuators: the test-masses are so maintained relatively motionless with a better accuracy than 10^{-11} m. In that way, the stability of the test-mass/instrument configuration limits the fluctuations of the parasitic forces applied on the mass due for instance to the gravity field gradients or the electro-magnetic field. It benefits also to the operation linearity of the instrument capacitive sensing and electrostatic actuations, mainly depending on the configuration geometry. The common applied electrostatic acceleration will be nullified by acting the satellite thrusters in such a way that the common instrument reference frame is following the two masses in their in orbit motion. The difference of the applied electrostatic acceleration will be accurately observed in the direction of the Earth gravity monopole to be analysed as an eventual Equivalence Principle violation signal.

So, the two test-masses are the two proof-masses of two concentric ultra-sensitive inertial sensors composing a differential accelerometer, called SAGE (Space Accelerometer for Gravitational Experimentation). MICROSCOPE satellite can operate two SAGE instruments that will be identical except the mass materials. The two materials used for the test will be a Platinum Rhodium alloy, PtRh10 (90% Pt, 10% Rh), and a Titanium alloy, TA6V (90% Ti, 6% Al, 4% Va). The selection of these materials takes into account both instrument performance concerns (homogeneity, accuracy of machining, stability, electrical and magnetic properties...) and theoretical test aspects (see Table 1). A significant difference in subatomic particles may increase the likelihood of a detectable EP violation: Damour and Blaser mention parameters to be considered like baryon number over the atomic mass $(N+Z)/\mu$, the neutron excess $(N-Z)/\mu$, and nuclear electrostatic energy in $Z(Z-1)/(N+Z)^{1/3}$ (Damour and Blaser 1994).

The second SAGE instrument includes two masses made of the same Pt-Rh alloy. This instrument is only devoted to the in orbit verification of the systematic experiment errors. Pt-Rh alloy has been preferred for its high density, leading to a better rejection of the spurious surface effects. This second instrument exhibits so a better precision than the first one with test-masses of different composition: confidence in the obtained result is mandatory in such experiment, that is why we have not selected another pair of masses with different composition.

The MICROSCOPE satellite is scheduled to be launched in 2012. The selected quasi-circular heliosynchronous orbit has an altitude of 810 km. This altitude, h, is a compromise between the $1/(R+h)^2$ gravity signal, the residual atmospheric density that may disturb the satellite motion and the satellite thrusters and launcher possibilities. The heliosynchronism leads to a fixed satellite Sun side and so to an optimised rigid solar panel configuration: a maximum power is delivered for a minimum size and, more important, the fixed thermal external conditions of the satellite are very favourable for its thermo-elastic behaviour and its internal fluctuations of temperature.

The one year mission consists in different instrument calibration and measurement sequences. In orbit, the symmetry of the electrostatic actuations on the masses will be verified to a relative level of about 10^{-4} in order to reject common motion disturbances. The off-centring of the masses, limited to less than 20 μm by construction, will be also surveyed to limit the gravity gradient effects. Sequences with inertial and rotating pointing of the satellite are considered. In the first case, the Earth gravity field is modulated along the test-mass axes, at the orbital frequency, i.e. $f_{EPi} = 1.7 \times 10^{-4}$ Hz. In the second case, it is modulated at the sum of the orbital frequency and the satellite spin rate, i.e. f_{EPs}. Two spin rates and two 90° phases of the satellite pointing versus the Earth, defined at the ascendant node of the orbit, will be considered. So, the heterodyne detection of an eventual EP violating signal will be performed at these frequencies (EP frequencies). A minimum of 20 orbits integrating period is considered for the rejection of the stochastic disturbing signals.

Other space missions aiming at the test of the Equivalence Principle are under study and proposed to be selected in the future. Among them, the STEP mission, leaded by Stanford University is proposed to NASA and ESA in the frame of an international cooperation (Mester et al. 2001). This mission, much more ambitious than MICROSCOPE, envisages the implementation of four superconductive differential accelerometers, and so four pairs of test-masses, inside a 2 K Helium Dewar: superconducting loops insure the very steady passive magnetic levitation of the masses and SQUIDs devices are exploited in specific differential circuits to perform the measurement of the actual common and relative motions of the test masses which are not servo-controlled. The thermodynamic instrument noise is reduced by the operating temperature allowing an expected EP test accuracy of 10^{-18}. This accuracy is very demanding with respect to the instrument and satellite production and operation, which is, as it is shown hereafter for the MICROSCOPE mission, already at the limit of the state of the art of many spacecraft technologies. Another mission, called Galileo Gallilei (Nobili et al. 2000), takes advantage, like in MICROSCOPE, of room temperature capacitive position sensing but considers the rotation of the test masses at rather high frequency, a few Hz, in order to better decouple their relative motion to the satellite disturbances in presence of mechanical spring between them, contrarily to MICROSCOPE. A laboratory model of the instrument is also developed to assess on ground the instrument concept and configuration.

Beside the scientific objectives of the MICROSCOPE mission, it remains, by its experiment relative simplicity and by its already demonstrated technologies with presently nine accelerometers in orbit (on board CHAMP, GRACE and GOCE satellites), a fine preparatory program for more ambitious space tests with a limited risk.

The major scientific instrument outputs are derived from the applied electrostatic forces on each test-mass which are accurately measured: $\overrightarrow{\Gamma}_{App,k}$, for the test-mass k (centre O_k) can be expressed according to the acceleration of the mass, the Earth gravity field acceleration and the resultant of the parasitic forces induced by the environment (depicted in Sect. 5):

$$\overrightarrow{\Gamma}_{App,k} = \frac{\overrightarrow{F}_{el_k}}{m_{Ik}} = \overrightarrow{\gamma}(O_k) - \frac{m_{Gk}}{m_{Ik}}\overrightarrow{g}(O_k) - \frac{\overrightarrow{F}_{pa_k}}{m_{Ik}} \tag{1}$$

Table 2 Main specifications of the satellite attitude control in the two operating modes, inertial and rotating pointing; in addition the drag compensation system limits the linear acceleration measured by the inertial sensors in common mode; both controls are performed by actuating the satellite micro-thrusters according to the outputs delivered by the 6-axes inertial sensors and the star trackers

	Stochastic signal	At DC (inertial s/c – rotating s/c)	At EP frequency (inertial s/c – rotating s/c)
Pointing	$0.6 - 0.2$ mrad/Hz$^{1/2}$	$2.5 - 2.5$ mrad a priori $1.0 - 1.0$ mrad a posteriori	$10 - 10$ µrad a priori $6 - 1.0$ µrad a posteriori
Angular velocity Ω	1×10^{-4} -1×10^{-6} rads^{-1} Hz$^{-1/2}$	1×10^{-6} $- \sim 4 \times 10^{-3}$ rads^{-1}	7×10^{-7} -1×10^{-9} rads^{-1}
Angular acceleration $d\Omega/dt$	5×10^{-9} -5×10^{-9} rads^{-2} Hz$^{-1/2}$	3×10^{-8} rads^{-2} over 20 orbits	1×10^{-11} -5×10^{-12} rads^{-2}
Linear acceleration	3×10^{-10} -3×10^{-10} ms^{-2} Hz$^{-1/2}$	3×10^{-8} ms^{-2} over 20 orbits	10^{-12} ms^{-2}

with m_I and m_G the inertial and gravitational mass: $\frac{m_{Gk}}{m_{Ik}} = 1 + \delta_k$. Let us recall that the Eötwös parameter for two test-masses k and l is defined by: $2\frac{|\delta_k - \delta_l|}{\delta_k + \delta_l}$.

So, the optimisation of the instrument consists in limiting all disturbances on the test-mass motion, especially about the EP test frequency and phase (or identical on both masses), predicting the exact (or the same) gravity field integrated on both masses, measuring the exact electrostatic force applied on it (amplitude, frequency and direction). The acceleration of each test-mass can be then expressed by considering the satellite linear and attitude motion, (O_{sat}, M_{sat}):

$$\overrightarrow{\Gamma_{App,k}} = \overrightarrow{\gamma}\,(O_{sat}) + H_{In,COR}(\overrightarrow{O_{sat}O_k}) - (1+\delta_k)\,\overrightarrow{g}\,(O_k) - \frac{\overrightarrow{F}\,pa_k}{m_{Ik}} \tag{2}$$

with the operator H representing the sum of three dynamics effects to be controlled during the experiment: the inertia effect due to the satellite angular acceleration and velocity, both controlled by the satellite system (see Table 2), the Corriolis effect and the relative acceleration of the test-mass versus the instrument/satellite frame. The two letters are limited because of the stability of the silica instrument frame and the accuracy of the mass electrostatic servo-control to this frame with a stability of better than 10^{-16} ms^{-2} at EP frequencies.

$$\begin{aligned} H_{In,COR}(\overrightarrow{O_{sat}O_k}) &= \left[\overrightarrow{\dot{\Omega}} \wedge \overrightarrow{O_{sat}O_k} + \overrightarrow{\Omega} \wedge (\overrightarrow{\Omega} \wedge \overrightarrow{O_{sat}O_k})\right] + 2[\Omega]\,\overrightarrow{\dot{O}_{sat}O_k} + \overrightarrow{\ddot{O}_{sat}O_k} \\ &= [In]\overrightarrow{O_{sat}O_k} + 2[\Omega]\,\overrightarrow{\dot{O}_{sat}O_k} + \overrightarrow{\ddot{O}_{sat}O_k} \end{aligned} \tag{3}$$

The satellite undergoes the Earth gravity, as well as external surface forces $\overrightarrow{F}\,ext$ like the atmospheric drag and the radiation pressures and also the thrust of its propulsion system $\overrightarrow{F}\,th$.

$$\underbrace{\left(M_I + \sum_k m_{Ik}\right)}_{M_{Isat}}\overrightarrow{\gamma}\,(O_{sat}) = \overrightarrow{F}\,ext + \overrightarrow{F}\,th + \underbrace{\left(M_G + \sum_k m_{Gk}\right)}_{M_{Gsat}}\overrightarrow{g}\,(O_{sat}) \tag{4}$$

Then, the expression of each inertial sensor output is:

$$\begin{aligned}\overrightarrow{\Gamma_{App,k}} &= \frac{M_{Gsat}}{M_{Isat}}\overrightarrow{g}(O_{sat}) - (1+\delta_k)\overrightarrow{g}(O_k) + R_{In,COR}(\overrightarrow{O_{sat}O_k}) - \frac{\overrightarrow{F}\,pa_k}{m_{Ik}} + \frac{\overrightarrow{F}\,ext}{M_{Isat}} + \frac{\overrightarrow{F}\,th}{M_{Isat}} \\ &= \overrightarrow{\Gamma}_{App,k/sat} - \frac{\overrightarrow{F}\,pa_k}{m_{Ik}} + \frac{\overrightarrow{F}\,ext_{/sat}}{M_{Isat}} + \frac{\overrightarrow{F}\,th_{/sat}}{M_{Isat}} \end{aligned} \tag{5}$$

The detail of the instrument operation leads to introduce matrices of sensitivities dK_{ij}, alignments ($\theta_{ij} = -\theta_{ji}$) and couplings ($\eta_{ij} = \eta_{ji}$) between the axes, plus biases, b_{0k}, due to the read-out circuits, electrostatic disturbing forces corresponding to any differences between the measured and the actual ones and quadratic non linear terms:

$$\begin{aligned}\overrightarrow{\Gamma}_{mes,k} = \underbrace{\overrightarrow{b}_{0k}}_{bias} &+ \Big([1 + \underbrace{dK_{1k}}_{scale}] + \underbrace{[\eta_k]}_{coupl.}\Big) \cdot \underbrace{[\theta_k]}_{align.} \cdot \left(\overrightarrow{\Gamma}_{App,k/sat} + \frac{\overrightarrow{F}\,ext_{/sat}}{M_{Isat}} + \frac{\overrightarrow{F}\,th_{/sat}}{M_{Isat}}\right) \\ &+ \Big([1 + \underbrace{dK_{1k}}_{scale}] + \underbrace{[\eta_k]}_{coupl.}\Big) \cdot \left(-\frac{\overrightarrow{F}\,pa_{k/inst,k}}{m_{Ik}} - \frac{\overrightarrow{F}\,el,par_{k/inst,k}}{m_{Ik}}\right) + \underbrace{K_{2k}}_{quad}\,\Gamma\Sigma^2_{App,k/sat}\end{aligned} \tag{6}$$

The stability of the introduced parameters of the instrument is of high importance for the accuracy of the experiment. In addition, common contributions and differences in the measured signals for both test-masses have to be separated. The first is used by the satellite computer for the compensation of the satellite drag. The second provides the EP test measure.

$$\begin{cases} \Gamma_{mes,c} = \frac{1}{2}\left(\Gamma_{mes,1} + \Gamma_{mes,2}\right) \\ \Gamma_{mes,d} = \frac{1}{2}\left(\Gamma_{mes,1} - \Gamma_{mes,2}\right) \end{cases} \tag{7}$$

with:

$$\begin{aligned}\overrightarrow{\Gamma}_{mes,d} = \underbrace{\overrightarrow{b}_{0d}}_{bias} &+ \Big([1 + \underbrace{dK_{1c}}_{scale}] + \underbrace{[\eta_c]}_{coupl.}\Big) \cdot \overrightarrow{b}_{1d} \\ &+ \Big([1 + \underbrace{dK_{1c}}_{scale}] + \underbrace{[\eta_c]}_{coupl.} + \underbrace{[d\theta_c]}_{align.}\Big) \cdot \overrightarrow{\Gamma}_{app,d/sat} + \Big(\underbrace{[dK_{1d}]}_{scale} + \underbrace{[\eta_d]}_{coupl.}\Big) \cdot \overrightarrow{b}_{1c} \\ &+ \Big(\underbrace{[dK_{1d}]}_{scale} + \underbrace{[\eta_d]}_{coupl.} + \underbrace{[\theta_d]}_{align.}\Big) \cdot \left(\overrightarrow{\Gamma}_{app,c/sat} + \frac{\overrightarrow{F}\,ext_{/sat}}{M_{Isat}} + \frac{\overrightarrow{F}\,th_{/sat}}{M_{Isat}}\right) \\ &+ \frac{1}{2}\underbrace{K_{2i}}_{quad}\Gamma^2_{App,i/sat} - \frac{1}{2}\underbrace{K_{2j}}_{quad}\Gamma^2_{App,j/sat} + O(dK, d\eta, d\theta)^2\end{aligned} \tag{8}$$

with index c and d specifying common and difference of the considered parameter defined as for the measured acceleration, and with:

$$\overrightarrow{b}_{1k} = \left(-\frac{\overrightarrow{F}\,pa_{k/inst,k}}{m_{Ik}} - \frac{\overrightarrow{F}\,el,par_{k/inst,k}}{m_{Ik}}\right) \tag{9}$$

considered in the instrument frame like $\overrightarrow{b}_{0k}$

$$\Gamma_{app,d/sat} = \frac{1}{2}\underbrace{(\delta_2 - \delta_1)}_{\delta} g + \frac{1}{2}\left(T_{/sat} - In_{/sat}\right).\Delta_{/sat} \tag{10}$$

where T is the gravity gradient tensor (Earth and satellite source), I_n is defined in (3) and Δ the distance between the two masses, all terms to be minimised; the signal proportional to δ is the one to be detected;

$$\begin{aligned}\Gamma_{App,c/sat} = &\left(\frac{M_{Gsat}}{M_{Isat}} - \frac{1}{2}(2 + \delta_1 + \delta_2)\right)\overrightarrow{g}\,(O_{sat})_{/sat} \\ &- \frac{1}{2}[T]_{/sat}\left(\delta_1\overrightarrow{O_{sat}O_1} + \delta_2\overrightarrow{O_{sat}O_2}\right) - [T]_{/sat}\,\overrightarrow{O_{sat}O_M} \\ &+ \frac{1}{2}R_{In,COR/sat}\left(\overrightarrow{O_{sat}O_M}\right)\end{aligned} \tag{11}$$

with M the middle of O_1O_2.

The term in $\overrightarrow{\Gamma}_{App,c/sat} + \frac{\overrightarrow{F}_{ext/sat}}{M_{Isat}} + \frac{\overrightarrow{F}_{th/sat}}{M_{Isat}}$ is fully rejected, only when the sensitivities, alignments and couplings of both sensors are matched. That is why the satellite drag-free system must minimise this term in presence of residual instrument asymmetries. *Fth/sat* is then managed by the drag-free servo-loop control to maintain, in the satellite control bandwidth and especially in the measurement one:

$$\rho\,\overrightarrow{\Gamma}_{mes,i} + (1-\rho)\,\overrightarrow{\Gamma}_{mes,j} = \overrightarrow{\Gamma}_{resDF} + \overrightarrow{C} \tag{12}$$

with $0 \le \rho \le 1$ and $\overrightarrow{\Gamma}_{resDF}$, $\overrightarrow{C}$ respectively the residue of the servo-control and the acceleration to be followed, according to the linear combination of the two inertial sensor outputs (see specification in Table 2).

3 Satellite Configuration

The MICROSCOPE satellite is derived from Cnes MYRIADE cubic platform with five rectangular aluminium honeycomb panels and one launcher interface. All equipments are fixed on these lateral and upper panels and the payload case is integrated at the centre on the lower structure. Two symmetric solar panels with half a meter square of AsGA cells each are located on the topside of the satellite maintained in the orbital plane: limited sizes, fixed panels and fixed solar orientations should guarantee a soft microvibration environment (see Fig. 1). In addition no moving masses like tank carburant sloshing or operating reaction wheels have been accepted during the EP experiment phase. A finite element model of the self gravity of the satellite has also been computed, with 31800 elements, leading to a DC gravity field on each test-mass less than 6.5×10^{-10} ms^{-2} and fluctuations at the EP frequency in the test direction of less than 1.1×10^{-16} ms^{-2}.

The two opposite sides of the satellite, X_s (in the orbital plane), carries the propulsion system: twelve Cesium electrical microthrusters are presently considered as well as cold gas proportional thrusters. The first solution avoids 20 kg of tank mass but requires 50 W more electrical power, i.e. 50% more solar panel area. The resolution shall be better than 0.1 μN. The second solution requires on each side two symmetric sets of three pressurised Nitrogen

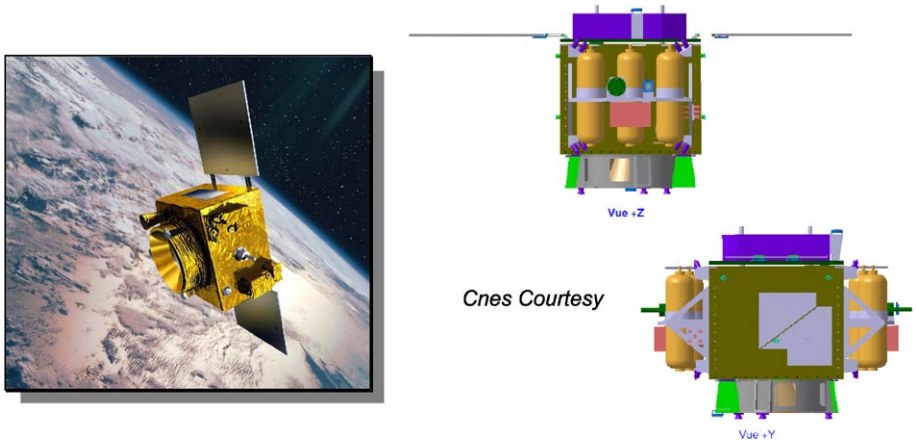

Fig. 1 The two satellite configurations with Field Effect Electrical Propulsion thrusters (*left*) or cold gas proportional thrusters (*right*), 150 μN maximum range each; the two opposite X_S panels carries the propulsion system; X_S, Y_S, axes are in the orbital plane, Z_S is the spin axis. The Cnes innovative control system compensates for the contact forces on the satellite, including atmospheric drag and radiation pressure, so that the satellite actually follows the two masses on their natural free-fall trajectory. The control system uses as input the linear and angular acceleration measurements from the two masses of the instrument under test, as well as the star trackers measurements

tanks compatible with the 5 mm positioning accuracy of the satellite centre of mass and the 1% inertia accuracy: many disturbing sources have been analysed to ensure this solution, like self gravity gradients, temperature and thermal gradients, centrifugal acceleration, gas convection and consumption, piezo-servo valves motions... All effects are maximised by 10^{-16} ms^{-2} (André et al. 2007).

The payload is composed of three units, the sensor unit (SU), the functional electronics unit (FEU) and the interface and control unit (ICU). The later manages the power supply of the instrument and the experiment processes, it interprets the telecommands and delivers the instrument data to the satellite bus. The two others require high thermal stability in order to meet high geometrical and electrical stability of the instrument arrangement, reduced radiometer and radiation pressure disturbances and electronics stability. They are mounted in a finally insulated two stage structure made in titanium with multi layer envelopes. The power consumption stability of the instrument is better than 5 mW for the electronics and one hundred times better for the sensor itself. So, a passive thermal control is compatible with the required stabilities, respectively:

- 1 mK for the tone fluctuations of the temperature, at the EP frequencies, f_{EPi} or f_{EPs}, for the second stage on which are mounted the inertial sensor heads at the satellite centre; and stochastic fluctuations of 0.3 KHz$^{-1/2}$ from 0.1 mHz to 0.1 Hz;
- 5 mK/m at f_{EPi} (2 mK/m at f_{EPs}) for the tone fluctuations of the thermal gradient of the same second stage; and 3 K/mHz$^{-1/2}$ from 0.1 mHz to 0.1 Hz in the axial direction;
- 10 mK at f_{EPi} (3 mK at f_{EPs}) for the tone fluctuations of the first stage on which are mounted the functional electronics and 1 KHz$^{-1/2}$ from 0.1 mHz to 0.1 Hz for the stochastic fluctuations.

Expected tone fluctuations of temperature are even lower when the satellite is rotating and with an EP frequency at least four times larger.

The first stage is only conductively linked to its own external radiator, pointing anti-sun and protected from the Earth flux instabilities by a 54 cm diameter baffle. Because the star trackers and the inertial sensors measurements are jointly exploited on board, in the satellite attitude estimator, and also on ground, in the a posteriori data correction, the star trackers are fastened on the same anti-sun panel in order to obtain a fine alignment stability of its view cone axis with respect to the instrument spin axis.

4 Instrument Concept and Design

The MICROSCOPE instrument of the EP test experiment is mainly composed of four space inertial sensors operating at finely stabilised room temperature and associated by pairs constituting two differential accelerometers (Touboul et al. 2002). The sensor unit (SU) of each accelerometer comprises two quasi cylindrical and co-axial masses inside two concentric silica cores which are integrated in the same vacuum tight housing (see Fig. 2). At the top of the housing, a getter pumping device maintains during the entire mission the residual pressure level, P_g, of less than 10^{-5} Pa. All parts inside are backed out before integration to reduce their outgazing. At the bottom, a pair of three moving fingers clamps the two masses during the launch in order to sustain the vibrations. In orbit, the pyrotechnic valve of the blocking mechanism opens its pressurised reservoir and release the spring that move out the fingers.

Each test-mass is so surrounded by two gold coated silica cylinders with cuts away of the gold for defining six pairs of electrodes which are used for both, the capacitive sensing of the position and attitude of the mass, and the servo-loop control of its six degrees of freedom (see Fig. 3). The distance between the mass and the cylinders is 600 µm corresponding to a difficult compromise between on one hand, the capacitive sensing resolution and the capacity of control of the electrostatic actuators and, on the other end, the reduction of the electrical test-mass disturbances induced for instance by contact potential differences.

The four quadrant electrodes of the inner cylinder allows the control of the radial axes: two translations, Y_i and Z_i, and two rotations about these axes. The cylindrical electrodes of the outer cylinder are symmetrically positioned around each end of the mass for the control

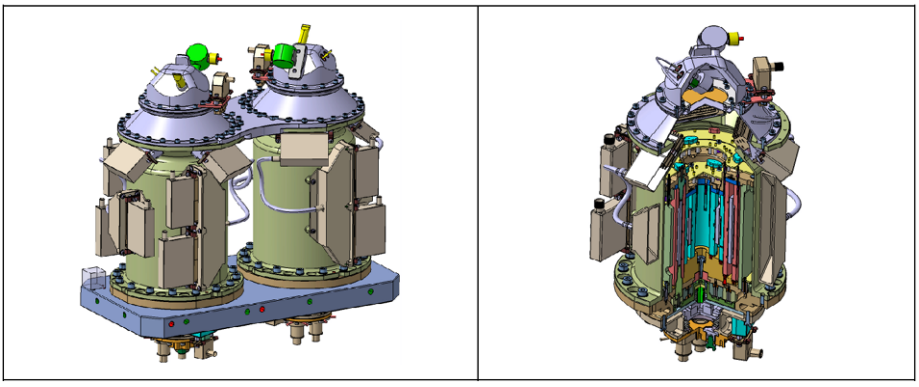

Fig. 2 Two twin sensor units are integrated at the centre of the MICROSCOPE satellite; the two tight housing (*left*) includes at the top the vacuum getter system and at the bottom the blocking mechanism of the masses; each one includes two concentric quasi-cylindrical test-masses surrounded by their gold coated silica core constituting two inertial sensors (*right*)

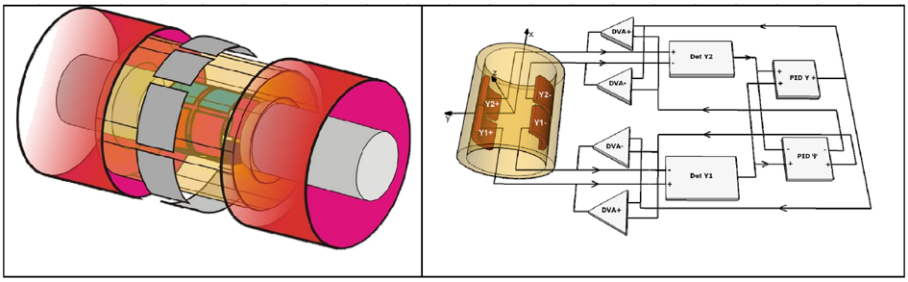

Fig. 3 *Left*—Electrode configuration of one sensor unit: the mass *(in yellow)* includes an inner silica cylinder with four pairs of quadrant electrodes (*in blue* and *red*) devoted to the radial test-mass control; the outer gold coated cylinder supports two cylindrical electrodes (*in pink*) at the ends of the mass and four pairs of electrodes at the centre (*in green*) in regard to the flat areas for the axial control. *Right*—As an example, the two servo-loops associated to the two pairs of electrodes for the control of Y_i and the rotation about Z_i

of the X_i axis. The EP test is performed along this axis that is optimised to exhibit the best accuracy with a reduced electrostatic stiffness due to difference of electrical potentials between the mass and the electrode cylinders. The rotation of the mass about its axis of revolution, X_i, is measured by the last pair of electrodes: in fact, this pair is distributed all around the mass with eight quadrants in regard to four flat areas in order to break the symmetry of revolution of the mass. The width of these flat areas is a compromise between the accuracy of the capacitive sensing and the importance of the gravitational multi-poles of the mass.

The two silica electrode cylinders of the inner mass are finely grinded and represent the reference frame of the first inertial sensor. Cylindricity of the parts, better than 3 μm, and concentricity, better than 5 μm, are demanded. Great care is also paid to position and align them with respect to the two others for the outer mass.

When the inertial sensor is on, its test-mass is electrostatically levitated at the centre of its cage without any mechanical contact. Each capacitive sensor is maintained at null, i.e. the capacitances between the mass and the two electrodes are identical: a 100 kHz sine wave pumping signal, V_d, is applied to the mass and the collected signals on each electrode are compared. Six channels including digital controllers generate from the six capacitive sensing outputs the opposite electrical voltages V_i which are applied on the opposite electrodes. Cold damping of all degrees of motion is provided in addition to a very accurate mass positioning (Grassia et al. 1999).

The electrical charge of the test-mass has to be controlled, in particular because of the high energy protons fluxes bombarding in orbit the satellite. That is why a thin gold wire of 5 μm diameter is used to fix the mass electrical potential to the electronics reference voltage: the stiffness and the damping factor of the wire have been carefully analysed and measured (Willemenot and Touboul 1999a, 1999b). Then, this wire is also used to apply on the mass the 100 kHz detection signal and a 5 V biasing voltage V_p: in presence of a perfect symmetric geometrical configuration and an anti-symmetric electrical one around the mass, the applied electrostatic force is proportional to V_p and to V_i. By measuring V_i, one can deduce forces and torques applied to the mass, which is maintained motionless to the cage. So, the difference of acceleration and gravity applied to the test-mass is obtained and also the angular acceleration of the instrument.

The already mentioned FEU box includes the capacitive sensing of both of the masses, the reference voltage sources and the analogue electronics to generate the electrical voltages applied on the electrodes. The ICU comprises the digital electronics associated to the control

Table 3 Local gravity gradient in the neighbourhood of the centres of the test-masses: this tensor can only be considered for very weak displacement about this centre

Gravity gradient (s^{-2})			
T_{ij}	X_i	Y_i	Z_i
X	-9.15×10^{-7}	-2.19×10^{-8}	1.72×10^{-9}
Y	-2.19×10^{-8}	6.09×10^{-7}	-1.30×10^{-9}
Z	1.72×10^{-9}	-1.30×10^{-9}	3.06×10^{-7}

laws of the servo-loops and the interfaces to the data bus of the satellite. It includes also the power converters.

The test-mass characteristics are major parameters for the success of the experiment. The geometry is machined with an accuracy of 1.5 μm by means and procedures developed in Physikalisch-Technische Bundesanstalt, Braunschweig, Germany. The material shall not include any non homogeneity larger than 5×10^{-5} and the shape is selected to present a spherical matrix of inertia with a relative accuracy of 5.3×10^{-6} for the inner mass and 2×10^{-6} for the outer mass, out of diagonal component being less than 2.6×10^{-6}. In addition, the gravity multipoles are compatible with a weak sensitivity to the change of the nearest masses distribution due to thermoelastic behaviour of the surrounded parts. These effects have been computed with finite elements representation of the overall two accelerometers package with 128 286 elements for the instrument and 3840 mass points for the test-mass. The computed DC gravity field along X_i, Y_i, Z_i is respectively (-9.92×10^{-9} ms^{-2}, 1.95×10^{-08} ms^{-2}, -1.39×10^{-10} ms^{-2}). More important are the gravity gradients (see Table 3) and their fluctuations with temperature.

Sensitivities of the difference of the instrument gravity field, applied on each test-mass, have been evaluated, first to the relative mass position and rotation: sensitivities are less than 2.9×10^{-7} ms^{-2}/m and 3.1×10^{-10} ms^{-2}/rad leading respectively to differential perturbations at the EP frequencies of 1.8×10^{-18} ms^{-2} and 8.7×10^{-20} ms^{-2} when considering the expected temperature fluctuations. Displacement of one sensor with respect to the other has also been considered leading to a maximum of 5.7×10^{-19} ms^{-2}. Dilatations of the parts introducing larger asymmetries have also been considered and leads in the worst case configuration to a maximum perturbation of 2.5×10^{-16} ms^{-2}. Improvement in the selection of the material (from invar to titanium) should even lower this value.

The magnetic susceptibility of the selected material, χ_m, is limited, 2.8×10^{-4} for Platinum alloy and 1.4×10^{-4} for titanium one, but requires nevertheless a sufficient shielding with respect to the Earth and satellite magnetic field fluctuations at EP frequencies. We have so evaluated, from the data of the Oersted space mission, the fluctuations of the Earth field that may be encountered along the orbit. We have in addition considered the worst case of the residual magnetic momentum of the MICROSCOPE satellite, i.e. 1 A m^2 with tone fluctuations at f_{EP} of 10^{-3} A m^2 and stochastic variations of 4×10^{-2} A m^2 Hz$^{1/2}$ at 0.3 m distance from the masses. We have computed the efficiency of the μmetal specific shield enclosing a large volume with both accelerometers in order not only to reduce the magnetic field but also its gradients. In complement, the sensor tight housing made in invar constitutes also a magnetic shield.

$$(\overrightarrow{\Gamma}_{m_{in}} - \overrightarrow{\Gamma}_{m_{out}}) \cdot \overrightarrow{X}_i = \frac{\chi_{m_{in}}}{2\mu_0 \cdot \rho_{m_{in}}} \overrightarrow{\nabla} \left[(\overrightarrow{B_{s/c}} + \overrightarrow{B_{Earth}})^2_{in} \right] \cdot \overrightarrow{X}_i - \frac{\chi_{m_{out}}}{2\mu_0 \cdot \rho_{m_{out}}} \overrightarrow{\nabla} \left[(\overrightarrow{B_{s/c}} + \overrightarrow{B_{Earth}})^2_{out} \right] \cdot \overrightarrow{X}_i \quad (13)$$

In these conditions, the differential applied acceleration along the EP axis, X_i, is evaluated depending on the cross product of DC and EP frequency harmonics of both residual fields of the Earth and the satellite. In the worst case configuration, when the DC residual magnetic moment of the satellite is along Y_i, a maximum difference of acceleration of 2.08×10^{-16} ms^{-2} is obtained in inertial pointing of the satellite; and 1.19×10^{-17} ms^{-2} in case of rotating satellite when the DC residual magnetic moment is along X_i.

5 Instrument Performances

The performances of the electrostatic inertial sensors depend on: (i) the parasitic forces and damping applied on the test-masses; in absence of electrostatic control, the mass is not fully in free fall; (ii) the electronics noise and bias drifts to be considered through the transfer functions of the servo-loops; the mass is then not perfectly controlled motionless to the instrument frame and so to the other one; (iii) the performance of the pick-up electronics to extract, digitalise and store the measurement signal; the measured signal is not fully representative to the applied control acceleration with the right sensitivity.

Radiometer effects, involving residual low pressure gas and temperature gradients, as depicted first by Einstein (1924), and radiation pressures have been over-estimated according to the specified temperature gradients of the instrument gold coated silica cage surrounding the masses along the considered axis (see in Sect. 3, the thermal environment of the sensor; temperature to be considered here are inside the core, filtered out by the own instrument thermal inertia and insulation) by:

$$\Gamma_n = \frac{S}{m} \cdot \Delta T_{Si} \cdot \left(\frac{1}{2} \cdot \frac{P_g}{T} \oplus \frac{4\sigma}{3c} \cdot 4T^3 \right) \tag{14}$$

Tone radiation acceleration are evaluated in worst case to 1.2×10^{-16} ms^{-2} and radiometer to 7.9×10^{-17} ms^{-2} without considering any pressure re-equilibrium (Pollack et al. 2007). Outgassing of the parts has been also evaluated and leads to lower disturbances because of the selected materials and the backing of the parts.

Contact potential differences (CPD) between the mass and the silica coatings are also sources of DC force and fluctuations as well as asymmetries of the geometrical or electrical configuration around the mass. But fortunately, the mass is controlled motionless with respect to the silica cylinders, thus one only has to take into account the thermal and time variations at the EP test frequency and not in particular the DC values. This makes a large difference for the CPD which fluctuations are much smaller then their eventual DC patch. Variations of 15 $\mu\mathrm{V/K}$ and $(1 + 10^{-2}/f)$ $\mu\mathrm{V/Hz}^{1/2}$ have been considered from in orbit results of the GRACE accelerometers (Touboul et al. 2004; Flury et al. 2008): larger levels should not be compatible with the exhibited 10^{-10} $\mathrm{ms}^{-2}\,\mathrm{Hz}^{-1/2}$ and bias stabilities.

Stiffness and damping of the thin gold wire glued on the mass and the silica support are also considered and remains a major limitation of the inertial sensor performance.

Capacitive position sensing fortunately exhibits very high performance, of a few 10^{-11} $\mathrm{mHz}^{-1/2}$ depending on the electrical gain of the sensor and the geometrical configuration (Josselin et al. 1999). Details of the sensor characteristics are presented in Table 4 according to the mass and the considered axis. The back action of the sensor is also very important to be estimated. With 5 V detection signal on the mass, the induced electrostatic stiffness and force depend on the defects of symmetry of the electrostatic geometry and

Table 4 Position capacitive sensing characteristics: gains, resolutions and thermal sensitivities (**a**); Power Spectral Density (PSD) of the sensor outputs in case of 40 V/pF gain (**b**)

	Electronics detection gain (V/pF)	Physical detection gain (pF/μm or pF/mrad)	Global detection gain (V/m or V/rad)	Output noise ($V/Hz^{1/2}$)	Output noise ($pm/Hz^{1/2}$ or $nrad/Hz^{1/2}$)	Thermal Sensitivity (ppm/°C)
Outer mass						
X	40	6.49×10^{-3}	2.60×10^{5}	1×10^{-5}	38.5	500
y/z	5	6.06×10^{-2}	3.03×10^{5}	5×10^{-6}	16.5	500
Tetha/psi	5	9.54×10^{-1}	4.77×10^{3}	5×10^{-6}	1.05	500
Phi	80	1.24×10^{-1}	9.92×10^{3}	1.20×10^{-5}	1.21	500
Inner mass						
X	80	3.71×10^{-3}	2.97×10^{5}	1.20×10^{-5}	40.4	500
y/z	16	1.37×10^{-2}	2.19×10^{5}	6.50×10^{-6}	29.7	500
Tetha/psi	16	1.06×10^{-1}	1.70×10^{3}	6.50×10^{-6}	3.83	500
Phi	80	1.76×10^{-2}	1.41×10^{3}	1.20×10^{-5}	8.52	500

(a)

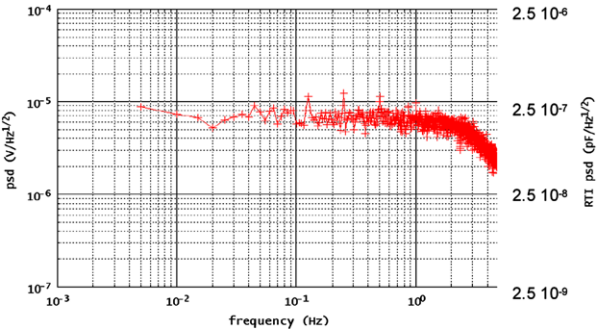

(b)

correspond, for the more sensitive outer mass and along the axial direction X_i, to a maximum noise of 8×10^{-15} $ms^{-2}\,Hz^{1/2}$ and a thermal drift of 7×10^{-14} ms^{-2}/K with respect to the electronics temperature and 1×10^{-14} ms^{-2}/K with respect to the sensor temperature.

For what concerns the electrostatic actuators, along the EP test axis, X_i, gains are respectively 3.25×10^{-8} ms^{-2}/V and 1.83×10^{-8} ms^{-2}/V for the outer and inner mass, the electrical noise of the electronics corresponding to 78.1×10^{-15} $N/Hz^{1/2}$ and 43.9×10^{-15} $N/Hz^{1/2}$.

The inertial sensor noise is so computed by quadratic sum of all stochastic contributions to the three above mentioned terms of the error budget. Figure 4 presents the obtained PSD of both sensors. At upper frequencies, the major contributor corresponds to the double derivation of the capacitive position sensing noise leading to $16 \cdot \pi^4 \cdot f^4 \cdot \mathrm{PSD}(x)$ law.

In the range from 10^{-3} to 10^{-2} Hz, read-out electronics noise of only 0.8 $\mu V/Hz^{1/2}$ have been obtained corresponding to 1×10^{-13} $ms^{-2}/Hz^{1/2}$ and CPD fluctuations are major contributors.

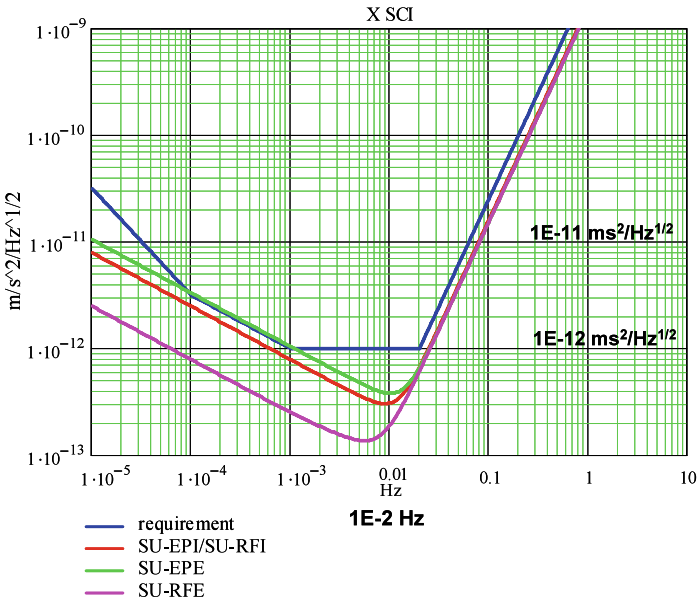

Fig. 4 $(PSD)^{1/2}$ expressed in $\mathrm{ms}^{-2}\,\mathrm{Hz}^{-1/2}$ of all inertial sensors: Platinum external mass (*in purple*), Platinum internal mass (*in red*), Titanium external mass (*in green*), objectives to be reached (*in blue*)

In the lower frequencies domain, Niquist fluctuation/dissipation due to gold wires is preponderant corresponding to $1/f$ PSD law (Willemenot and Touboul 1999b).

$$\Gamma_n = \frac{1}{m}\sqrt{4k_B T \cdot \frac{S}{2\pi f \cdot Q}} \tag{15}$$

with S, gold wire stiffness, evaluated to 3.8×10^{-8} N/m and quality factor Q to one hundred at the EP test frequencies. At frequencies much lower then the orbital frequency, thermal fluctuations become more important and correspond to $1/f^2$ PSD.

6 Experiment Systematic Errors and in Orbit Calibration

In addition to the stochastic errors that can be reduced by the integration of the measured signal or the number of the experiment sessions, systematic errors have been considered: they are eventual sine wave signals at same frequency and phase as the Earth point gravity projection on the test-mass axial direction. They are mainly due to thermal sensitivities of the electronics or of the instrument core associated with sine wave fluctuations of the temperature at the EP test frequency, f_{EP}. Magnetic field fluctuations have been already considered above and self gravity of the satellite and the instrument too. Earth gravity gradients are also major sources of systematic errors.

The instrument core benefits of a temperature environment stability of 1 mK at f_{EP}. In addition, inside the tight housing, parts are insulated: the response time of the levitated mass temperature is larger than 60 hours and of the silica core larger than 1 hour and half. In these conditions, the two major contributors are the fluctuations of the gold wire stiffness due to

the relative Yong Modulus sensitivity ($1/E \cdot dE/dT = 4 \times 10^{-4}$/K) and the variations of contact potential differences leading respectively to 1.6×10^{-16} ms^{-2} and 5×10^{-17} ms^{-2} disturbances. Tone fluctuations of the thermal gradient in the tight housing generate also systematic errors, respectively evaluated to 8×10^{-17} ms^{-2} for the radiometer effect and 1.2×10^{-16} ms^{-2} for the radiation pressure.

The 3 mK tone thermal variations of the electronics leads in particular to variations of the reference voltages applied on the mass, V_p at DC and V_d at 100 kHz. This corresponds, in presence of geometrical defects of symmetry of the mass or of the electrode parts, to 1.5×10^{-16} ms^{-2} tone error.

A direct sum of all these terms and others (not mentioned here but smaller) corresponds to an artefact signal of 6.2×10^{-16} ms^{-2} for the Titanium mass sensor and 2.9×10^{-16} ms^{-2} for the Platinum one with a full scale range of respectively 2.6×10^{-7} ms^{-2} and 2.3×10^{-7} ms^{-2}.

Thanks to the drag-free loop of the satellite, the instrument output is maintained at a mean null value to better than 10^{-8} ms^{-2}. So, the evaluated thermal variations of the instrument sensitivity, limited to less than 10^{-8}, do not introduce a major disturbance in addition.

Effects of the Earth gravity gradient, tensor $[T]$, requires beside the already mentioned characteristics of the masses, the centring of the two masses (see (10)). In fact, when considering only the Earth monopole, $[T]$ can be expressed in the instrument reference frame, and in the case of an inertial pointing satellite, by:

$$
\begin{aligned}
T_{11} &\approx \frac{1}{2}\frac{\mu}{R^3}\Bigg[1 + 3\cos(4\pi f_{orb}t) + e\Bigg(-\frac{3}{2}\cos(2\pi f_{orb}t - \psi) + 3\cos(2\pi f_{orb}t + \psi) \\
&\quad + \frac{21}{2}\cos(6\pi f_{orb}t + \psi)\Bigg)\Bigg] \\
T_{12} &= T_{21} \approx 0 \\
T_{13} &= T_{31} \approx \frac{1}{2}\frac{\mu}{R^3}\left[-3\sin(4\pi f_{orb}t) + e\left(\frac{3}{2}\sin(2\pi f_{orb}t - \psi) - \frac{21}{2}\sin(6\pi f_{orb}t + \psi)\right)\right] \\
T_{22} &\approx -\frac{\mu}{R^3}\left[1 + 3e\cos(2\pi f_{orb}t + \psi)\right] \\
T_{23} &= T_{32} \approx 0 \\
T_{33} &\approx \frac{1}{2}\frac{\mu}{R^3}\Bigg[1 - 3\cos(4\pi f_{orb}t) + e\Bigg(\frac{3}{2}\cos(2\pi f_{orb}t - \psi) + 3\cos(2\pi f_{orb}t + \psi) \\
&\quad - \frac{21}{2}\cos(6\pi f_{orb}t + \psi)\Bigg)\Bigg]
\end{aligned}
\tag{16}
$$

With R the orbit means radius and e, the orbit eccentricity. The major terms of $[T]$ are at DC and $2f_{orb}$. Nevertheless, the eccentricity creates a term at $3f_{orb}$ and overall at f_{orb}, i.e. the EP experiment frequency. Eccentricity is constrained by the launcher to less than 5×10^{-3} but not better. That is why the relative off centring of the two masses, Δ, less than 20 μm after careful integration, is not sufficiently weak to make this term negligible in the differential measurement (see (8)). The MICROSCOPE approach is so to evaluate in orbit the off centring along X_ι and Z_ι in order to correct the measurement with a model of the Earth gravity field. To do so, the a posteriori knowledge of the satellite position and attitude must be sufficiently accurate as well as the timestamp of the measurements. Due to uncertainties in the changes of reference frame between the instrument measurement

axes and the gravity gradient model corrections, the centring of the masses in the Y_i is also evaluated. Off-centrings can be measured in orbit, by the observation of the signal, either induced by $[T]$ at 2 f_{orb}, or induced by $[In]$ (see (3)) when the satellite is voluntarily excited in attitude at a calibration frequency (Guiu et al. 2007).

By biasing the attitude control and the drag compensation servo-loops of the satellite, linear or angular sine wave accelerations can be applied to the satellite via its propulsion system. This will be done during the in orbit calibration phase of the instrument that helps to match the sensitivity matrices of the sensors reducing in (8) the terms in $d\Theta_c$ and in dK_d and Θ_d.

Performances better than the following specifications have been demonstrated by simulations: $d\Theta_c(Y_i \text{ or } Z_i) < 10^{-3}$ rad; $dK_d < 1.5 \times 10^{-4}$; $\Theta_d \cdot (Y_i \text{ or } Z_i) < 5 \times 10^{-5}$ rad; $\Delta_y < 4$ µm; $(1 + dKc) \cdot \Delta < 0.1$ µm (X_i or Z_i).

The stability of these sensor characteristics is sufficient between two in orbit calibrations. The frequency of these calibration phases has been selected according to the long term temperature stability of the payload case depending on the orbital conditions. Corrections of the measurement files are performed on ground by taking into account the calibrated factors. Then the rejection of the common mode accelerations of the test-masses is improved and the differential accelerations reduced.

7 Mission Performance and Discussion

From (10) and (11), common mode and differential accelerations can be evaluated taking into account the satellite orbital and attitude motions and the instrument characteristics. First, the overall error budget of all six measurements of each sensor have been performed in such a way to verify the expected performance of the attitude and drag compensation system of the satellite, and also to take into account alignment and coupling between axes in the differential measurement. Then, the differential measured acceleration is evaluated at the EP frequency after the ground calibration: this measure includes or not the violating signal.

In the performed uncertainty analysis, worst case computations have been performed and stochastic errors are all summed quadratically while systematic errors are directly summed without considering statistic distributions of the amplitude and phase of the computed tone errors. More then two hundred terms have been evaluated.

For the stochastic errors, the first four error sources are summarised in Table 5 in the case of a rotating pointing satellite corresponding to f_{EP} frequency of about 8×10^{-4} Hz. The major term is due to Niquist noise introduced by the damping of the 5 µm diameter, 2.5 cm length gold wires between the masses and the instrument cages. This term is quite identical to the quadratic sum of all terms that is 1.48×10^{-12} ms^{-2} Hz$^{1/2}$. Increasing the frequency

Table 5 Four major stochastic errors of the MICROSCOPE EP test experiment

Terms in the equation of measure	PSD$^{1/2}$ at f_{EP}	Effects, sources
Differential accelerometer noise	1.40×10^{-12} ms^{-2} Hz$^{1/2}$	Mass damping
Bias sensitivity to SU thermal gradient	0.38×10^{-12} ms^{-2} Hz$^{1/2}$	Radiation & radiometer force
Satellite AOCS & mass off centring	0.24×10^{-12} ms^{-2} Hz$^{1/2}$	Centrifugal accelerations Diff.
Scale factor sensitivity to FEU temp.	0.13×10^{-12} ms^{-2} Hz$^{1/2}$	Voltage ref. source instability

Table 6 Six major systematic errors of the MICROSCOPE Equivalence Principle test experiment

Terms in the equation of measure	Tone error amplitude at f_{EP}	Effects, sources
Projection of diff. accel.	5.2×10^{-16} ms^{-2}	Instability of star tracker axis versus instrument axis
Scale matching & AOCS	5.0×10^{-16} ms^{-2}	Drag free residual acceleration
Bias fluctuations, b_1	4.0×10^{-16} ms^{-2}	Magnetic parasitic force fluctuations
Bias sensitivity to SU temp.	3.6×10^{-16} ms^{-2}	Gold wire stiffness thermal variations
Scale factor sensitivity to FEU temp.	3.1×10^{-16} ms^{-2}	Thermal fluctuations of the electrostatic actuator gains
Bias sensitivity to FEU temp.	2.8×10^{-16} ms^{-2}	Electrostatic configuration dissymmetry: thermal variations of the resultant pressure

of the EP test should reduce this term but the spin of the satellite is limited by the strength of the thrusters and the satellite centring.

The second term corresponds to thermal gradient noise inside the accelerometer cores which generate fluctuations of the radiation and radiometer forces. The third one is the effect of the residual angular acceleration noise of the satellite that is not identical on the two masses because of the off centring. The last one corresponds to the reference voltage thermal fluctuations: this is the reference of the whole electrostatic configuration around the mass and it contributes to the scale factor of the performed acceleration measurement.

Table 6 presents the major systematic errors, at the EP frequency and computed in a worst case approach. In fact the direct sum of all these errors leads to 4.81×10^{-15} ms^{-2}. This is a majoring value of the actual disturbance that could be interpreted as a 5σ occurrence (1σ value is then 0.96×10^{-15} ms^{-2}). All sine wave disturbing signals (more than fifty) should not be in the experiment at worst cases, so at maximum amplitudes, neither exactly at the same phase than the expected EP signal. For instance, the temperature of the sensor parts and the electronics components are submitted to fluctuations, with a contribution at EP frequency, but depending of the thermal flux propagations, not at the same phase. In addition, different EP test phases and frequencies are performed during the one year mission. By performing a quadratic sum of these systematic errors, a more reduced contribution is obtained, 1.17×10^{-15} ms^{-2}, this value seems to be coherent with the previous estimation of the 1σ error from the direct sum.

The first term corresponds to the instabilities of orientation of the sensor star trackers mounted on the satellite anti-sun face with respect to the instrument axes. The satellite structure is specifically rigid here but thermal gradients effects may introduce fluctuations of the orientations that will limit the rejection of the differential accelerations applied on both masses. The second term is introduced in the differential acceleration, Γd, by the remaining defects (after in orbit calibration and ground correction) in the sensor axes scale factor matching and alignment, leading to a contribution of the residual common mode acceleration which is not fully nullified by the satellite drag compensation system. The third is induced by the fluctuations of the residual magnetic field distribution, around the two masses exhibiting different volumes and susceptibilities. The forth is due to the thermal sensitivity of the gold wire stiffness, the mass being controlled at null of the electrostatic configuration and not at null of the wire spring. The two last mentioned terms correspond to the thermal fluctuations of the reference voltage V_p and V_d: in presence of a configuration asymmetry, these voltage fluctuations result in variations of electrostatic pressures on the test-masses

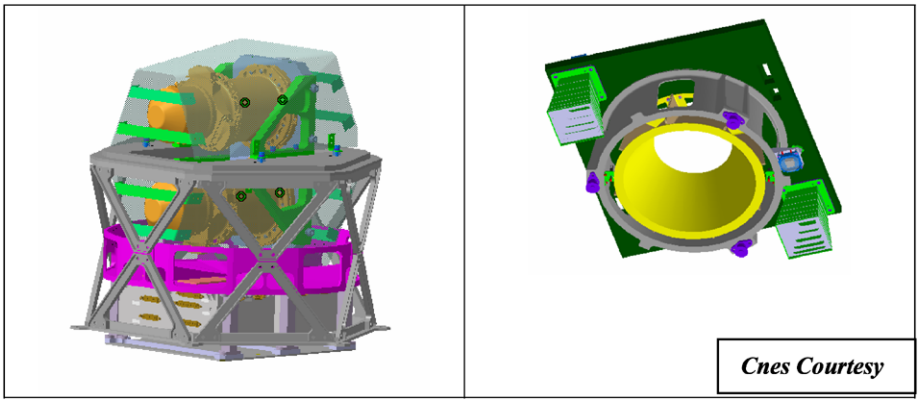

Fig. 5 Payload case (*left*) and bottom satellite plate (*right*); the two differential accelerometer including each two inertial sensor (*in gold*) are included inside the magnetic shield; the purple structure separates the accelerometers to the electronics unit; the bottom plate support the radiator for the electronics (not drawn here) at the centre of a conic baffle to protect it from the Earth radiation; the two sensor star trackers are mounted on the same plate

and variations of the gain of the electrostatic actuators. It appears clearly that the thermal behaviour of the payload case with its satellite bottom face, supporting the radiator with its baffle and the two star sensor trackers, is a key element of the experiment success. That is why, dedicated tests will be performed in the near future to assess the first obtained experimental results and calibrate the numerical thermal simulations.

By considering the duration (20 orbits) of one experiment session, the stochastic error corresponds to 4.3×10^{-15} ms^{-2} rms value (1σ), to be considered in addition to the systematic resultant error evaluation. This results in a total of 4.4×10^{-15} ms^{-2} or 6.4×10^{-15} ms^{-2} depending on the selected evaluation for the systematic error (quadratic or direct sum). This level must be compared to the in orbit Earth gravity at 810 km of about 8 ms^{-2}: EP test accuracy should be then from 0.55×10^{-15} to 0.80×10^{-15}.

By considering longer experiment sessions of 120 orbits, as it is presently the objective of the satellite operation, the total evaluated error is 2.1×10^{-15} ms^{-2} or 5.1×10^{-15} ms^{-2} corresponding to EP test accuracy of 0.26×10^{-15} and 0.64×10^{-15}. During the one year mission and in addition to the commissioning phase of the satellite and the instrument, at least fifty measurement sessions are presently foreseen in the in orbit experiment scenario. This is to the benefit of the rejection of the stochastic errors and to the characterisation of the instrument sensitivities and the systematic errors, in particular through the differential accelerometer including two test-masses made of the same Platinum alloy.

This uncertainty analysis shows that the present definition of the mission and the instrument are in agreement with the objectives of the test of the Equivalence Principle with 10^{-15} accuracy or better. Numerical simulations of the satellite operation agree with the specification of the attitude control and of the drag compensation. Electronics of the instrument have been tested and exhibits noise, bandwidth, gains and linearities in accordance. Prototype models of the instrument have been integrated with silica masses (small density) in order to be accurately tested in laboratory under one g. Operation and dynamics behaviour of the electrostatic servo-loops have been already verified, effort is now paid in a more detailed experimental analysis of the performance. In addition, free fall tests of the instrument are prepared with the ZARM drop tower facility in Bremen. This facility gives the opportunity to observe on board a capsule and during its 9 s vertical parabolic motion, the actual operation

of the four inertial sensors, in their flight configuration and in microgravity. Flight models of the accelerometers should be ready for the integration in the MICROSCOPE satellite in 2010 for a mission in the following years.

Acknowledgements This work was supported primarily by Onera, the French Aerospace Lab in Châtillon, France. The author would like to express his gratitude to the MICROSCOPE mission staff of Cnes in Toulouse, the Observatoire de la Côte d'Azur in Grasse and Onera in Châtillon, for all exchanges about the mission, the satellite and the payload. He is particularly grateful to G. Métris, A. Robert and R. Chhun for many discussions. The research described in this paper was carried out in Onera Châtillon, the development of the instrument is performed under contract with Cnes. MICROSCOPE is a Cnes mission with ESA cooperation.

References

Y. André et al., Impact de la propulsion gaz froid sur la mission MICROSCOPE. *Cnes Report* MIC-NT-S-0-962-CNS (2007)
S. Baessler et al., Improved test of the equivalence principle for gravitational self- energy. Phys. Rev. Lett. **83**, 18 (1999)
C. Brans, R.H. Dickes, Mach's principle and a relativistic theory of gravitation. Phys. Rev. **124**, 925 (1961)
D.G. Currie et al., A lunar laser ranging RetroReflector array for the 21st century, in *NLSI Lunar Science Conference* (2008)
T. Damour, Testing the equivalence principle: Why and how? Class. Quantum Grav. **13**, A33–A41 (1996)
T. Damour, J.P. Blaser, Optimizing the choice of materials in equivalence principle experiments, in *Particle Astrophysics, Atomic Physics and Gravitation*, ed. by J. Tran Than Van, G. Fontaine, E. Hinds (Frontières, Gif-sur-Yvette, 1994), pp. 433–440
T. Damour, F. Piazza, G. Veneziano, Violation of the equivalence principle in a dilaton-runaway scenario. Phys. Rev. D **66**, 046007 (2002)
A. Einstein, *The Meaning of Relativity* (Princeton University Press, Princeton, 1922) (1988)
A. Einstein, Theory of radiometer energy source. Z. Phys. **27**, 1–6 (1924)
D. Feldman, Z. Liu, P. Nath, Sparticles at the LHC. JHEP **04**, 054 (2008)
J. Flury, S. Bettadpur, B.D. Tapley, Precise accelerometry onboard the GRACE gravity field satellite mission. Adv. Space Res. **42**, 1414–1423 (2008)
F. Grassia et al., Quantum theory of fluctuations in a cold damped accelerometer. Eur. Phys. J. D **8**, 101–110 (1999)
E. Guiu et al., Calibration of MICROSCOPE. Adv. Space Res. **39**, 315–323 (2007)
G.D. Hammond et al., New constraints on short-range forces coupling mass to intrinsic spin. Phys. Rev. Lett. **98**, 081101 (2007)
L. Iorio, LARES/WEBER-SAT and the equivalence principle. Europhys. Lett. **80**, 40007 (2007)
V. Josselin, P. Touboul, R. Kielbasa, Capacitive detection scheme for space accelerometers applications. Sens. Actuators **78**, 92–98 (1999)
L. Lafargue, M. Rodrigues, P. Touboul, Towards low temperature electrostatic accelerometry. Rev. Sci. Instrum. **73**, 1 (2002)
J. Mester, R. Torii, P. Worden, N. Lockerbie, S. Vitale, C.W.F. Everitt, The STEP mission: principles and baseline design. Class. Quantum Grav. **18**, 2475–2486 (2001). See also http://einstein.stanford.edu/
R. Newman, Prospects for terrestrial equivalence principle tests with a cryogenic torsion pendulum. Class. Quantum Grav. **18**, 2407–2415 (2001)
A. Nobili et al., The GG project: Testing the Equivalence Principle in space and on Earth. Adv. Space Res. **25**, 1231–1235 (2000)
S.E. Pollack, S. Schlamminger, J.H. Gundlach, Outgassing, temperature gradients and the radiometer effect in LISA: a torsion pendulum investigation. arXiv:gr-qc/0702051v2 (2007)
G. Schäfer, Where do we stand in testing general relativity? Adv. Space Res. **32**(7), 1203–1208 (2003)
S. Schlamminger et al., Test of the equivalence principle using a rotating torsion balance. Phys. Rev. Lett. **100**, 04110 (2008)
T.J. Sumner et al., STEP (satellite test of the equivalence principle). Adv. Space Res. **39**, 254–258 (2007)
P. Touboul et al., MICROSCOPE, testing the equivalence principle in space. C. R. Acad. Sci. Paris, Sér. IV **2**, 1271–1286 (2001)
P. Touboul et al., The MICROSCOPE mission. Acta Astronaut. **50**(7), 433–443 (2002)
P. Touboul et al., In orbit nano-g measurements, lessons for future space missions. Aerospace Sci. Technol. **8**, 431–44 (2004)

C.M. Will, *Theory and Experiment in Gravitational Physics* (Cambridge University Press, Cambridge, 1985)
E. Willemenot, P. Touboul, On-ground investigations of space accelerometers noise with an electrostatic torsion pendulum. Rev. Sci. Instrum. **71**(1), 302–309 (1999a)
E. Willemenot, P. Touboul, Electrostatically suspended torsion pendulum. Rev. Sci. Instrum. **71**(1), 310–314 (1999b)
J.G. Williams, X.X. Newhall, J.O. Dickey, Relativity parameters determined from lunar laser ranging. Phys. Rev. D **53**, 6730 (1996)